Available online at www.sciencedirect.com
SCIENCE DIRECT®
Acta Materialia 52 (2004) 2701–2710
Acta MATERIALIA
www.actamat-journals.com

Segregation of hydrogen at internal Ag/MgO (metal/oxide)-interfaces as observed by small angle neutron scattering

C. Kluthe [a,*], T. Al-Kassab [a], J. Barker [b], W. Pyckhout-Hintzen [c], R. Kirchheim [a]

[a] Georg-August-Universität Göttingen, Institut für Materialphysik, Tammanstraße 1, 37077 Göttingen, Germany
[b] NIST, Center for Neutron Research, Gaithersburgh, MD, USA
[c] FZ Jülich, Institut für Festkörperforschung, Germany

Received 21 July 2003; received in revised form 11 February 2004; accepted 12 February 2004
Available online 12 March 2004

Abstract

The chemical composition of metal/oxide (M/O)-interfaces was studied for an internally oxidized Ag–1at.%Mg-alloy with small MgO nanoprecipitates in a dilute Ag matrix. This composition was varied by exposing the sample to oxygen ($p(O_2) = 2 \times 10^4$ Pa), hydrogen ($p(H_2) = 10^5$ Pa) or vacuum ($p < 10^{-4}$ Pa). By means of small angle neutron scattering (SANS) we were able to show that hydrogen segregates at the internal Ag/MgO-interfaces. The average hydrogen occupancy at the Ag/MgO-phase boundary can be determined to be $\Theta_H = (7.1 \pm 0.5) \times 10^{14}$ H/cm^2. In addition it could be shown that for each segregated hydrogen atom one Ag atom is displaced from the M/O-interface. The amount of hydrogen at the interfaces is in agreement with a model of structural vacancies at densely packed interface planes. To the best of our knowledge these are the first SANS-measurements that provide information about the segregation of hydrogen and deuterium at internal interfaces.

Keywords: Small angle neutron scattering; Hydrogen in metals; Oxides; Interface segregation; Core shell model; Metal/oxide-interfaces

1. Introduction

Metal-ceramic (M/C) interfaces are of great technological interest within the fields of dispersion hardening, nanostructured materials, coatings and microelectronics. For the technical application of M/C-composites, the mechanical properties of the interfaces are especially important. A sufficient understanding of the mechanical properties of the M/C-interface becomes essential for the welding of M/C-components or applying ceramic protective coatings on metals. The segregation of gases, e.g. oxygen or hydrogen, at these interfaces may influence their chemical structure and hence result in a modification of the material properties. It is well known for instance that the hydrogen embrittlement of high strength steels with small carbide precipitates is due to the segregation of hydrogen at the internal iron/carbide-interfaces with concomitant formation of microcracks [1]. In a different context, the segregation of gases at internal interfaces is interesting and auspicious concerning a possible application of such systems as hydrogen storage media. Therefore, it is necessary to understand the atomic structure of M/C-interfaces and their segregation behavior for hydrogen. Using high resolution electron microscopy (HREM) and analytical field ion microscopy (FIM), metal/oxide (M/O)-interfaces produced by internal oxidation have been investigated during the last decade [2,3]. The internal oxidation of a homogeneous binary alloy can be considered from a thermodynamic point of view as a phase decomposition in a ternary A–B–O-system. If a binary alloy AB, consisting of a noble metal A with small additions of less noble metal B, is annealed under oxygen at high temperature, then only metal B will be oxidized. In addition, for $c_O \cdot D_O \gg c_B \cdot D_B$, where c_O is the solubility of oxygen, c_B the concentration of B, and D_O, D_B are the diffusion coefficients of oxygen and solute B, respectively, an oxide BO_n precipitates within the A-matrix, which becomes

* Corresponding author. Tel.: +49-551-395-028; fax: +49-551-395-012.
E-mail address: ckluthe@ump.gwdg.de (C. Kluthe).

1359-6454/$30.00 © 2004 Acta Materialia Inc. Published by Elsevier Ltd. All rights reserved.
doi:10.1016/j.actamat.2004.02.018

diluted in B [4]. This case is termed internal oxidation. At low temperatures nanosize BO_n precipitates may be formed and, therefore, a large amount of M/O-interfacial area can be produced within a small sample volume.

Various systems of oxide particles within a noble metal matrix, produced by internal oxidation, e.g. Ag/CdO and Nb/Al_2O_3 [2], were investigated using HREM. By means of HREM imaging of the interfaces the authors concluded, that the terminating (1 1 1)-interface of the investigated oxide consists of oxygen only (and not Cd or Al). Using electrochemical methods, it could be shown for the Pd/MgO-system that, after internal oxidation at high oxygen pressures, both reversible and irreversible trapping of hydrogen were found after H-charging of the samples [5]. After ultra high vacuum (UHV)-annealing of the samples, only a reversible trapping behavior of hydrogen was found. To describe these results the following structural model has been developed by Huang et al. [5]: assuming the oxide (e.g. MgO) has a perfect stoichiometry and the interface has no additional (image) charge, the (1 1 1)-interface of the oxide consists of 50% structural vacancies within the terminating oxygen layer (Fig. 1(a)). The authors suggest that if the system is annealed under high oxygen pressure, additional so-called excess-oxygen is able to segregate into the vacancies of the (1 1 1)-interface (Fig. 1(b)). According to Huang et al. [5] the segregated excess-O has the same bonding state as the terminating oxygen corresponding to the stoichiometric interface. The excess-O can be treated as the amount of oxygen which segregates above the stoichiometry of MgO at the M/O- interface. However, it should be noticed that the terminating oxygen atoms of the oxide are indistinguishable from the excess-oxygen atoms. In order to become an O^{2-}-ion, a charge transfer occurs between the terminating oxygen and the adjacent more noble Ag-atoms resulting in an Ag–O bond. The terminating oxygen atoms then form a weak bond to the matrix atoms and do not only belong to the oxide precipitate. This simplified picture is supported by analytical transmission electron microscopy (TEM)-studies [6–8] revealing the presence of Ag–O or Cu–O (for MgO precipitates in Cu) at the interface after annealing treatments at high oxygen partial pressures ($p(O_2) = 2 \times 10^4$ Pa). In addition, the presence of excess-O enables hydrogen to be bound at the interface, if the system is doped with hydrogen (Fig. 1(b)). The interfacial hydrogen leads effectively to a change in the interfacial bond-pattern and implies the formation of strong O–H bonds at the interface, while the electron density between O and Ag interfacial atoms strongly decreases or even vanishes.

Since this structural model should be valid for all M/O-interfaces produced by internal oxidation we expect a similar trapping of H by excess-O for the Ag/MgO-system. For larger MgO-precipitates within the grain boundaries the evidence of this excess-O has been proved recently by Pippel et al. [8] using electron energy loss spectroscopy (EELS). The occupancy of this excess-O at (1 1 1)-particle interfaces was determined by means of gas volumetry to be 2.2×10^{14} cm^{-2} [9]. Since MgO is a very stable oxide and silver is a noble metal with the highest oxygen diffusivity, the internal oxidation of a binary Ag–1at.%Mg-alloy can be performed at low temperatures leading to smaller oxide precipitates providing a larger amount of M/O-interfacial area than in any other internally oxidized system. For instance the amount of the total M/O-interfacial area for the system Pd/MgO is by a factor 10-100 smaller than for the system Ag/MgO for the same sample dimensions. MgO-precipitates in Ag produced by internal oxidation were already analyzed by 3D-atom probe (3DAP) [10]. A detailed investigation of this system indicates that nearly mono-dispersal distribution of MgO-precipitates are produced, with a mean radius ranging from 0.5 up to 2.5 nm depending on the preparation parameters (oxidation temperature and annealing time) [11]. The width of the size distribution decreases from $\sigma/R = 0.3$ for the early stages to $\sigma/R = 0.2$ for the later stages, where R is the mean particle radius and σ is the standard deviation of the size distribution.

Up to now the segregation of solute atoms in a dilute matrix has been investigated using indirect methods, e.g. where the effect of a reduced diffusivity or activity was studied [11]. In cases, where strong segregation takes place a direct observation of segregation by TEM/EELS is possible [12,13]. With the exceptional spatial resolution and high elemental sensibility of the 3D-atom probe (3DAP), segregation of B to an edge dislocation has been revealed in three dimensions [14]. With the same

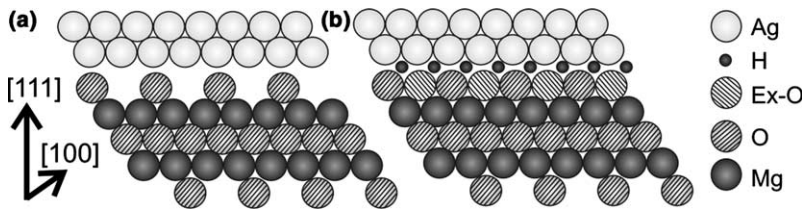

Fig. 1. Structural Model of the M/O-interface according to Huang et al. [5]. (a) Stoichiometric (1 1 1)-interface exhibiting structural vacancies after annealing in UHV, zone axis [1 1 0]. (b) Interfacial excess-O occupies the structural vacancies upon annealing under high oxygen pressures ($p(O_2) = 2 \times 10^4$ Pa). Hydrogen can form a strong bond to this excess-O, if the system is doped with hydrogen.

method, the segregation of Ag at MgO- and Sb at CdO-precipitates in Cu- and Ag-matrix, respectively, have been investigated [15,16].

A somewhat different approach to determine segregation of hydrogen and deuterium to MgO-particle interfaces in Ag is small angle neutron scattering (SANS). This method has been applied successfully to the segregation of hydrogen and deuterium at dislocations in palladium and vanadium [17–19]. In contrast to the microscopic technique, SANS averages over a large volume. Analytical tools such as EDX and EELS are not applicable for a solute like hydrogen. In addition, it is very difficult to study solute segregation by TEM in a region less than 1 nm. Depending on the decomposition pressure of the system, the hydrogen may also escape into the vacuum. In 3DAP-analysis, hydrogen may be detected if the analysis is done at very low temperatures less than 50 K and a homogeneous field evaporation of the specimen is achieved. Otherwise, residual gases (mainly hydrogen) will be adsorbed at the specimen and theses gases appear in the 3DAP-analysis. Unfortunately, the field evaporation of MgO-precipitates in silver is not homogeneous [20]. As a result, hydrogen is detected in the mass spectra of the analysis, although the specimens were not charged with hydrogen [20].

The advantage of SANS is the large scattering cross-section of hydrogen and deuterium for neutrons. The different sign of the coherent scattering length of H and D enables the observation of the segregation at the M/O-interface and rules out other scattering contributions by contrast variation experiments.

2. Expected scattering laws

The scattered intensity is usually expressed by the macroscopic scattering cross-section $\mathrm{d}\Sigma/\mathrm{d}\Omega(Q)$ as

$$\frac{\mathrm{d}\Sigma}{\mathrm{d}\Omega}(Q) = N\left|\int \Delta\rho \exp(-\mathrm{i}Qr)\,\mathrm{d}^3r\right|^2, \tag{1}$$

where N is the number of the scattering objects, $\Delta\rho$ the difference of the scattering length densities, i.e. number of scattered atoms times their coherent scattering length b_n per unit volume and Q as scattering vector. An evaluation of Eq. (1) for the special case of a normalized macroscopic scattering cross-section $\mathrm{d}\Sigma/\mathrm{d}\Omega|^0_{\mathrm{Layer}}(Q)$ of a segregated layer around a particle is given in Appendix A. For the Guinier-regime, the following approximation for $\mathrm{d}\Sigma/\mathrm{d}\Omega|^0_{\mathrm{Layer}}(Q)$ is obtained:

$$\left.\frac{\mathrm{d}\Sigma}{\mathrm{d}\Omega}\right|^0_{\mathrm{Layer}}(Q) = \frac{\left.\frac{\mathrm{d}\Sigma}{\mathrm{d}\Omega}\right|_{\mathrm{P+L}}(Q) - \left.\frac{\mathrm{d}\Sigma}{\mathrm{d}\Omega}\right|_{\mathrm{P}}(Q)}{\left.\frac{\mathrm{d}\Sigma}{\mathrm{d}\Omega}\right|_{\mathrm{P}}(Q)} = \frac{6\Delta\rho_{\mathrm{L}}\delta R}{\Delta\rho_{\mathrm{PM}}R}\cdot\exp\left(-\frac{Q^2R^2}{15}\right), \tag{2}$$

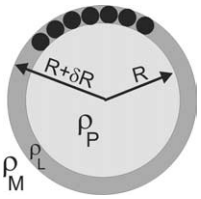

Fig. 2. Schematic illustration of a spherical particle P of radius R covered with a spherical shell L of thickness δR. The scattering length densities of the different components are ρ_{M} for the matrix, ρ_{L} for the shell and ρ_{P} for the particle.

where R is the particle radius and δR the thickness of the layer (see Fig. 2). $\Delta\rho_{\mathrm{PM}}$, $\Delta\rho_{\mathrm{L}}$ are the differences of the scattering length densities of the particle to matrix and segregated layer to vacuum. The normalized net cross-section $\mathrm{d}\Sigma/\mathrm{d}\Omega|^0_{\mathrm{L}}(Q)$ of the layer is the ratio of the difference between the cross-section $\mathrm{d}\Sigma/\mathrm{d}\Omega|_{\mathrm{P+L}}(Q)$ of a sample loaded with hydrogen (deuterium) and the scattering cross-section $\mathrm{d}\Sigma/\mathrm{d}\Omega|_{\mathrm{P}}(Q)$ of an uncharged sample divided by the latter.

Two unknown parameters appear in Eq. (2), the layer thickness δR and the scattering contrast $\Delta\rho_{\mathrm{L}}$ of the layer. Assuming that hydrogen segregates at the particle interfaces without affecting the density of the interface atoms in its vicinity, the scattering contrast $\Delta\rho_{\mathrm{L}}$ is given according to its definition by

$$\Delta\rho_{\mathrm{L}} = \frac{N_{\mathrm{H}}\cdot b_{\mathrm{H}}}{V} = \frac{N_{\mathrm{H}}\cdot b_{\mathrm{H}}}{A\cdot\delta R} = \frac{\Theta_{\mathrm{H}}\cdot b_{\mathrm{H}}}{\delta R}, \tag{3}$$

where N_{H} is the number of segregated H-atoms in volume V with corresponding coherent scattering length b_{H}. Θ_{H} is the occupancy of hydrogen at the interface given in cm^{-2}. Then the product $\Delta\rho_{\mathrm{L}}\delta R$ in Eq. (2) with its two unknowns is replaced by the product $\Theta_{\mathrm{H}}b_{\mathrm{H}}$ with only one unknown, i.e. the hydrogen coverage Θ_{H}.

During the interpretation of the experiments, it turned out that the results for H- and D-doped samples were not consistent with the developed model, because the ratio of normalized cross-sections of hydrogen and deuterium did not yield the ratio of the correspondinng scattering length (i.e. $b_{\mathrm{H}}/b_{\mathrm{D}}$) as predicted by Eqs. (2) and (3). A similar inconsistency was discovered for H- and D-segregation at dislocations in Pd [19], where it was overcome by assuming a change of the Pd-density as a consequence of H-enrichment and associated lattice expansion. Presuming that hydrogen affects the matrix density in the vicinity of the interface by displacing Ag-atoms, an additional contribution has to be taken into account

$$\Delta\rho_{\mathrm{L}} = \frac{\Theta_{\mathrm{H}}\cdot b_{\mathrm{H}} - \Theta_{\mathrm{Ag}}\cdot b_{\mathrm{Ag}}}{\delta R}, \tag{4}$$

where Θ_{Ag} is the amount of Ag-atoms displaced per cm^2 interface and b_{Ag} the coherent scattering length of Ag. Hence, if a displacement of Ag-atoms takes place due to the segregation of H, the layer contrast $\Delta\rho_{\mathrm{L}}$ is

diminished by the second term in Eq. (4). Due to the negative sign of the coherent scattering length of H ($b_H = -3.74$ fm, $b_D = +6.67$ fm), segregation of hydrogen increases the absolute contrast, whereas the scattering contrast is diminished by deuterium. The stronger coherent scattering of D compared to H is reduced, if the segregation of H (D) at the M/O-interface is accompanied by a dilution of Ag-atoms.

To calculate the change of the Ag-density, at first, the H-occupancy density Θ_H has to be determined. Otherwise, Eq. (4) consists of two unknown parameters. To calculate Θ_H it is possible to use the different signs of b_D and b_H in a contrast variation experiment. In addition, it is reasonable to assume that $\Theta_H = \Theta_D$, because H and D are chemically identical. A subtraction of the normalized net cross-section of H and D under use of Eqs. (2) and (4) leads to

$$\left.\frac{d\Sigma}{d\Omega}\right|^0_{D-H}(Q) = \left.\frac{d\Sigma}{d\Omega}\right|^0_{D}(Q) - \left.\frac{d\Sigma}{d\Omega}\right|^0_{H}(Q) = \frac{6\Theta_H(b_D - b_H)}{\Delta\rho_{PM}R}\exp\left(-\frac{(QR)^2}{15}\right). \quad (5)$$

The particle size R can be evaluated from SANS-measurements of the uncharged samples. Hence, the H-occupancy is the only unknown parameter in Eq. (5) and can be easily calculated from the axis intercept in a modified Guinier-plot of $\ln R \cdot d\Sigma/d\Omega|^0_{D-H}(Q)$ versus $(QR)^2$.

3. Experimental

The Vacuumschmelze GmbH Hanau kindly provided the Ag–1at.%Mg-alloy. This alloy was cold rolled to thin foils of 150 μm thickness. The samples were recrystallized in order to suppress the formation of larger MgO-precipitates within grain boundaries. The formation of the oxide particles is enhanced at grain boundaries, owing to the even faster diffusion of oxygen at these boundaries. After annealing at a temperature of 923 K for 4 days under argon atmosphere ($p(O_2) < 0.2$ Pa, $p(H_2O) < 10^{-2}$ Pa) an average grain size of 100 μm was attained. The samples were then etched in a dilute solution of H_2O_2 and NH_3 to remove any oxide layers and to ensure a homogeneous oxidation. The internal oxidation was performed in dry air at temperatures of 1023–1123 K and between 3 and 21 days. Precipitates of 1–5 nm diameter are formed within the Ag matrix under these conditions [10]. The size distribution of the oxide particles was characterized by means of the 3DAP. After internal oxidation, the samples were slowly cooled down in the furnace to avoid quenching of oxygen in the Ag-matrix. Finally, the surface of the samples was electropolished using a mixture of perchloric and acetic acid (1:10) at 8 V DC. A platinum electrode was used as a cathode. Doping the SANS samples was done from the gas phase under 1 bar H_2 or D_2, respectively, at 663 K for 7 h. Afterwards the samples were slowly cooled down to room temperature with constant pressure. Under these conditions we expect the maximum amount of hydrogen at the M/O-interfaces within the samples.

Prior SANS measurements on the systems Cu/MgO and Ag/MgO were performed at the Forschungszentrum Jülich, Germany, using the small angle diffractometer KWS1. Most of the SANS measurements, which are presented in this paper, were performed at the National Institute of Standards and Technology, Gaitersburgh, MD, at the NG-7 30 m small angle scattering instrument. The distance between sample and detector was chosen to be 1 and 3.45 m in order to cover the range of $Q = 0.012$–0.66 Å^{-1}. A sample aperture of 19 mm was used. The 2D-data of the detector was radially averaged and the incoherent background contribution mainly arising from hydrogen was subtracted.

4. Results

Fig. 3 shows a typical scattering curve of an uncharged, internally oxidized Ag–1at.%Mg-sample. A Q^{-4}-dependence is observed for all samples at lowest Q-values. According to Porod [21], this scattering is stemming from particles with sharp interfaces and a total interfacial area S per unit sample volume. It is described by the following approximation:

$$\frac{d\Sigma}{d\Omega}(Q) = \frac{2\pi \cdot S \cdot \Delta\rho^2_{PM}}{Q^4}. \quad (6)$$

Assuming that the observed particles are MgO, the total M/O-interfacial area $S = 10^2$–10^3 cm^2/cm^3 is calculated using the corresponding contrast $\Delta\rho_{PM}$ (Table 1). As the

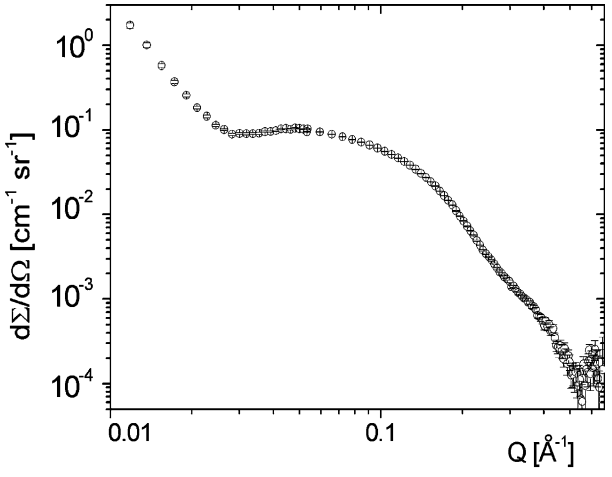

Fig. 3. SANS-scattering curve of an internally oxidized Ag–1at.%Mg-sample. The particle radius of the MgO-precipitates is $R = (1.82 \pm 0.06)$ nm.

Table 1
Values of MgO-particles inside the Ag-grains evaluated from SANS data

T_{IO}/t_{IO}	v (10^{-2})	$R_{Guinier}$ (nm)	$R_{Modul.}$ (nm)	S (10^5 cm^{-1})	S_{GB} (10^2 cm^{-1})
923 K/1 d	0.83 ± 0.01	0.88 ± 0.01	0.91 ± 0.07	7.81 ± 0.05	–
1023 K/1 d	0.85 ± 0.01	1.06 ± 0.01	1.09 ± 0.06	5.66 ± 0.05	–
1023 K/14 d	0.65 ± 0.01	1.27 ± 0.01	1.27 ± 0.08	4.93 ± 0.05	–
1023 K/21 d	0.76 ± 0.07	1.61 ± 0.05	1.59 ± 0.14	3.74 ± 0.04	10.1 ± 0.8
1073 K/ 21 d	0.71 ± 0.07	1.82 ± 0.06	1.78 ± 0.12	3.11 ± 0.04	8.6 ± 0.2
1123 K/ 3 d	0.76 ± 0.07	2.17 ± 0.08	2.15 ± 0.19	2.82 ± 0.04	9.8 ± 0.7
1098 K/ 21 d	0.70 ± 0.06	2.28 ± 0.08	2.28 ± 0.15	2.24 ± 0.03	3.4 ± 0.2

S_{GB} is the M/O-interface of the oxide particles within the grain boundaries. T_{IO} is the oxidation temperature and t_{IO} the annealing time.

Porod law is valid for $Q < 0.01$ A^{-1}, the particles have to be larger than 60 nm. According to TEM-investigations, the MgO-particles in the grain boundaries have a mean diameter of ~100 nm [8,22]. Results from TAP-investigations of this system show that the mean diameter of the MgO-particles inside the Ag-grains is 1–5 nm. Therefore, the Porod-scattering at small Q is most probably stemming from larger MgO-particles located at grain boundaries. At larger Q-values, first a plateau is observed, which is followed by a Q^{-4}-dependence (Fig. 3). These are the Guinier and the Porod-regime of the smaller MgO-precipitates located inside the Ag-grains. For particles with spherical symmetry, the following approximation is fulfilled for the Guinier-regime:

$$\frac{d\Sigma}{d\Omega}(Q) = \frac{4}{3}\pi \cdot v \cdot R^3 \Delta\rho_{PM}^2 \cdot \exp\left(-\frac{Q^2R^2}{5}\right). \quad (7)$$

The volume fraction v and the particle radius R of the MgO precipitates could be determined from the Guinier scattering by plotting $\ln d\Sigma/d\Omega(Q)$ versus Q^2 (see Fig. 4).

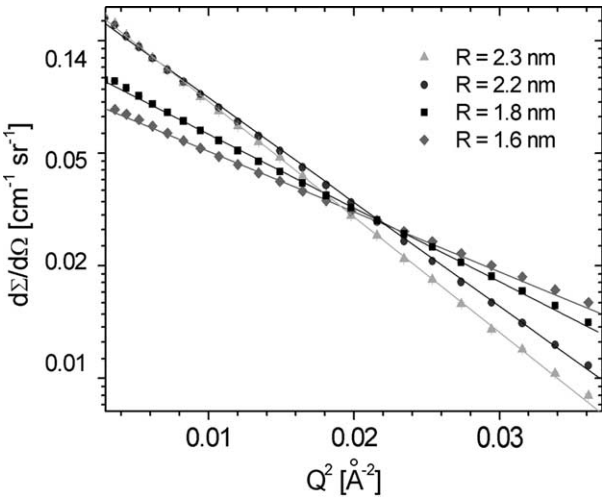

Fig. 4. Gunier plots of the macroscopic scattering cross-section for Ag–1at.%Mg-samples after internal oxidation. The radii compiled in the inset were obtained from the slope of the straight lines via Eq. (7) and are presented in Table 1. The slopes are obtained by least square fits of the data points within the linear region.

In addition, all scattering curves of the uncharged samples show modulations at larger Q-values due to a rather narrow size distribution of the MgO-particles within the Ag-grains. The modulations come from the scattering of a sphere (see Eq. (A.5)). Therefore, the particle size could also be evaluated from the modulations and could be compared with the one calculated from the Guinier-regime. The total M/O-interfacial area S of these smaller precipitates can be calculated from the Porod-scattering at larger Q-values. All values determined by these different evaluation procedures for the uncharged samples are shown in Table 1.

As can be seen in Table 1, the internal oxidation of a binary Ag–1at.%Mg-alloy leads to nano-precipitates of MgO with a mean particle radius of 0.88–2.28 nm depending on the oxidation parameters. The size of the precipitates increases with the oxidation temperature T_{IO} and the time of the internal oxidation treatment. The values for the particle size calculated by the Guinier approximation and from the modulation of the sphere form factor are nearly identical. Moreover, the values determined by SANS are in agreement with previous TAP-investigations of this system. For further evaluation of the data, the particle size obtained from Guinier-scattering were used, due to their smaller error bars. The volume fraction v of small MgO-precipitates in Table 1 is smaller than the expected value of 0.011 due to the large precipitates at grain boundaries. Though the larger MgO-precipitates within the grain boundaries possess a volume fraction of ~30–40% of all MgO within the sample, their contribution to the total M/O-interfacial area can be neglected. The fraction of the smaller MgO-precipitates of the total M/O-interfacial area is more than 99%.

The values of the interfacial area S obtained from the Porod-regime should obey the following relation:

$$S = N4\pi R^2 = \frac{3v}{R}. \quad (8)$$

As can be seen in a plot of S versus R^{-1}, the data are in good agreement with the relationship expected by Eq. (8) (Fig. 5).

Fig. 6 shows the scattering cross-section of samples charged with H, D and of the uncharged sample in a

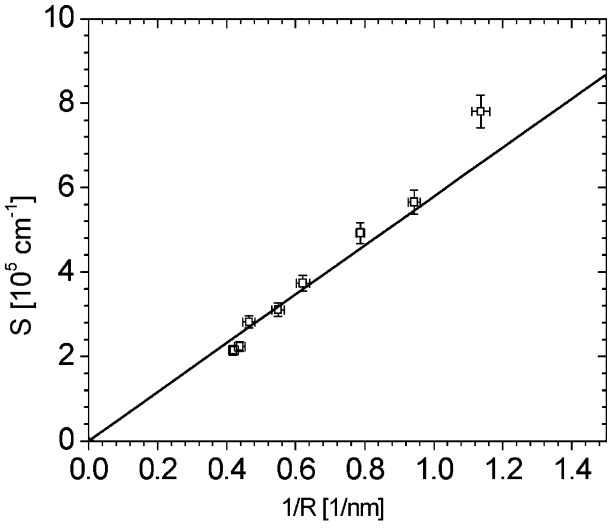

Fig. 5. Plot of total interfacial area S versus R^{-1}. The straight line represents the expected line through the origin.

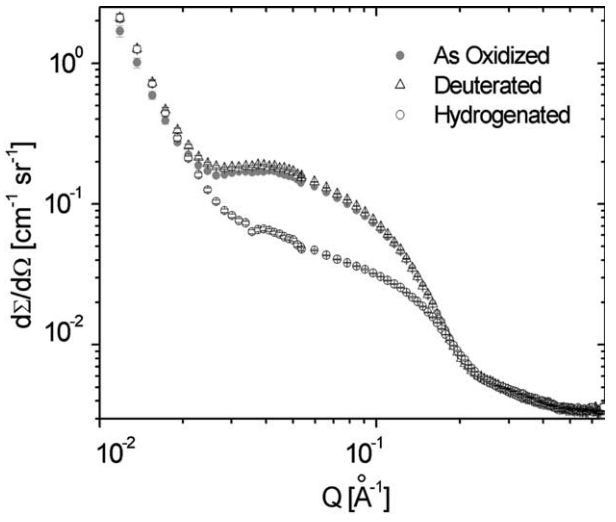

Fig. 6. Double logarithmic plot of the scattering cross-section of uncharged, H- and D-charged internally oxidized Ag–1at.%Mg-samples with a mean particle radius of $R = (2.17 \pm 0.08)$ nm.

double logarithmic plot of $d\Sigma/d\Omega(Q)$ versus Q. All samples had an identical size distribution with a mean particle radius of $R = (2.17 \pm 0.08)$ nm. Within the Guinier-regime the sample charged with D has a higher intensity (~15%) compared to the uncharged sample, whereas the intensity decreases (~70%) after H-charging a sample of the same stock. The changes of $d\Sigma/d\Omega$ due to H (D)-charging can be more clearly seen in a semi logarithmic plot (see Fig. 7) with $R = (1.61 \pm 0.05)$ nm. As will be shown in the following, this strong effect on $d\Sigma/d\Omega(Q)$ due to H (D)-charging can only be explained by a segregation of hydrogen (deuterium) to the M/O-interfaces of the sample. These changes due to H (D)-charging did not disappear, even after an annealing of the samples in high vacuum (~10^{-4} Pa) at 773 K. This

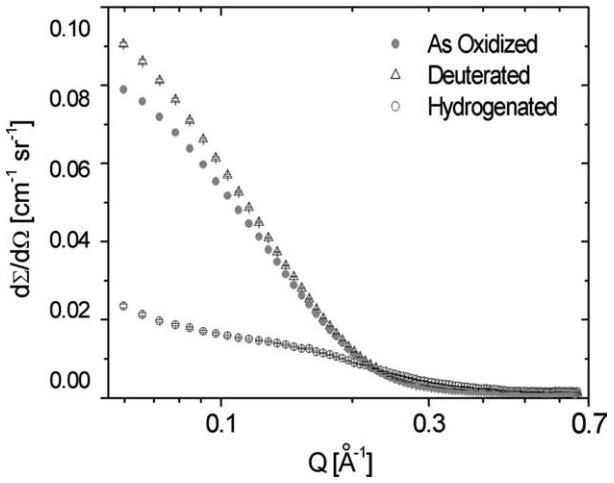

Fig. 7. Semi-logarithmic plots of $d\Sigma/d\Omega(Q)$ of an uncharged, H- and D-charged internally oxidized Ag–1at.%Mg-sample with a mean particle radius of $R = (1.61 \pm 0.05)$ nm.

indicates that hydrogen is irreversibly trapped within the sample at this temperature and pressure.

All scattering curves of samples charged with hydrogen had a higher background compared to the uncharged samples due to the strong incoherent scattering of hydrogen. From this incoherent background at larger Q-values, the H-concentration could be determined according to

$$c_H = \left.\frac{d\Sigma}{d\Omega}\right|_{inc.H} \cdot \frac{4\pi \cdot V_{Ag}}{\sigma_{inc}^{H}}, \tag{9}$$

where c_H is the fraction of sites occupied by hydrogen, $d\Sigma/d\Omega|_{inc.H}$ is the incoherent scattering cross-section of the H-charged sample, V_{Ag} the atomic volume of Ag and $\sigma_{inc}^{H} = 80.27$ barn the incoherent cross section of H ($\sigma_{inc}^{D} = 2.05$ barn, $\sigma_{inc}^{Ag} = 0.58$ barn, $\sigma_{inc}^{MgO} = 0.035$ barn).

The normalized net cross-section (after Eq. (2)) is shown in Fig. 8. The decrease in $d\Sigma/d\Omega(Q)$ due to

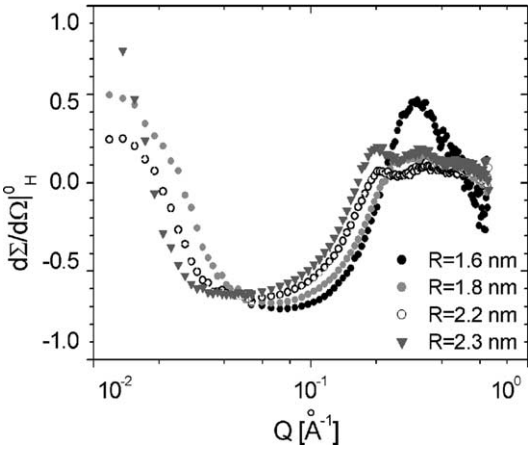

Fig. 8. Normalized scattering net cross-section of an H-doped sample in a semi-logarithmic plot. The net cross-section $d\Sigma/d\Omega|_{Layer,H}(Q)$ increases in absolute value within the Guinier-regime ($Q \sim 0.1$ Å^{-1}) with decreasing size of the MgO-particles.

H-charging becomes more distinct for smaller MgO-particles. This is consistent, because smaller oxide particles represent a larger amount of total M/O-interfacial area than larger particles (see Fig. 5). In Fig. 9, the normalized scattering cross-section is presented in a modified Guinier plot. According to Eq. (2), straight lines can be fitted to the data points within the Guinier-regime and the product $\langle \Delta\rho_L \delta R \rangle_H$ of the shell contrast $\Delta\rho_L$ and shell thickness δR of a segregated layer of H can be evaluated from the intercept with the ordinate. According to Eq. (2), the mean value of this contrast product is calculated as $\langle \Delta\rho_L \delta R \rangle_H = -640 \pm 73$ cm^{-1}. In an analogous manner $\langle \Delta\rho_L \delta R \rangle_D = 80 \pm 15$ cm^{-1} is calculated for deuterium. Thus the contrast product of hydrogen is significantly higher than in the case of deuterium. Since the shell thickness and the occupancy should be identical for H and D, this result must be explained in terms of an additional contribution to the shell contrast according to Eq. (4). This additional contribution decreases the contrast for deuterium, but increases the contrast for H (in absolute magnitude).

It is possible to determine the hydrogen occupancy density Θ_H by contrast variation. An H/D-contrast variation can be performed for samples with equal size distributions of their MgO-particles. Because H and D are chemically identical, $\Theta_H = \Theta_D$ is fulfilled. The contrast variation experiments were performed for two samples with two different mean MgO-particle sizes. According to Eq. (5), the occupancy density Θ_H could be evaluated from the axis intercept of a modified Guinier-plot (Fig. 10). The mean value of the occupancy density of hydrogen (and deuterium) is

$$\Theta_H = (7.1 \pm 0.5) \times 10^{14} \text{ cm}^{-2}.$$

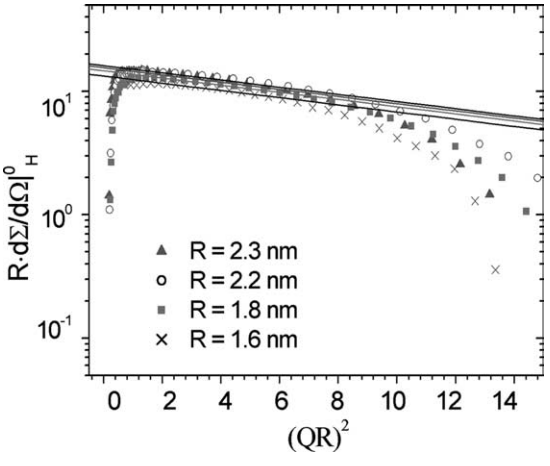

Fig. 9. Modified Guinier-Plot of $\ln R \cdot d\Sigma/d\Omega|_L(Q)$ versus $(QR)^2$ according to Eq. (2) of H-charged Ag/MgO-samples. The straight lines with a slope −1/15 correspond to fits according to Eq. (2) within the Guinier-regime. The contrast of the segregated layer is obtained from their axis intercepts.

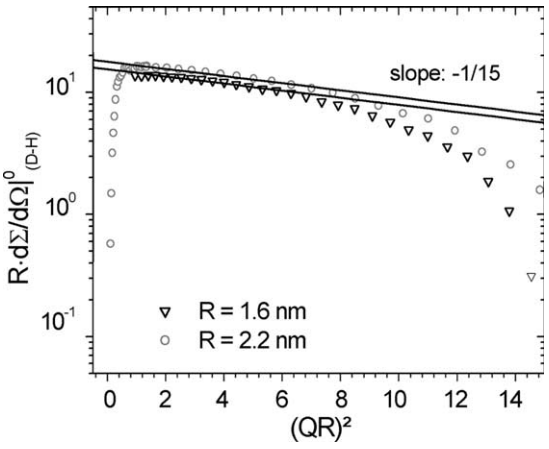

Fig. 10. Modified Guinier-plot of the difference of the normalized net cross-sections of D and H after Eq. (5). The straight lines correspond to fits within the Guinier-regime according to Eq. (5). The hydrogen occupancy density Θ_H is received from the axis intercept.

This amount is equal to half a monolayer of hydrogen at the Ag/MgO-particle interface. With knowledge of the hydrogen occupancy Θ_H and the contrast product $\langle \Delta\rho_L \delta R \rangle$ for H and D, it is possible to calculate the change of the matrix density (due to segregation) via Eq. (4)

$$\Theta_{Ag} = (6.4 \pm 1.3) \times 10^{14} \text{ cm}^{-2}.$$

When comparing the calculated value of Θ_{Ag} with Θ_H it is obvious that for about each segregated H-atom one Ag-atom is displaced from the M/O-interface.

5. Discussion

Since the hydrogen solubility in pure silver ($c_H(Ag) \sim 10^{-14}$ H/Ag at 296 K) and MgO is negligible [24], a certain solubility of an internally oxidized Ag–1at.%Mg-system, which means pure MgO precipitates in a pure Ag-matrix, can only be explained by the segregation of hydrogen at the Ag/MgO-particle interfaces. This presumption can be verified by comparing the H-concentration with the total number of hydrogen traps at the M/O-interface. The total number of hydrogen atoms trapped can be determined from the coherent scattering (Eq. (10))

$$c_H^{\text{Interf.}} = \frac{\Theta_H \cdot S_{MgO}}{N_{Ag}} \tag{10}$$

with $N_{Ag} = 5.846 \times 10^{28}$ Ag/m^3 and $\Theta_H = 7.1 \times 10^{18}$ H/m^2. S_{MgO} is the total M/O-interface of the sample (Table 1). Assuming that the matrix solubility is negligible and all hydrogen of the sample is located at the M/O-interfaces, the value evaluated according to Eq. (10) has to be equal to the H-concentration of the sample. The hydrogen concentration can be determined

from the incoherent scattering at large Q-values (Eq. (9)). As can be seen in Table 2, both values are about the same within their error bars. In addition, the hydrogen concentration increases for smaller particles due to their larger total interfacial area. Therefore, all hydrogen of the sample has to be located at the M/O-interfaces.

As stated above, the scattering behavior of a H-doped sample remains the same even after annealing at 773 K for 1 h in high vacuum (HV) ($\sim 10^{-4}$ Pa). Since the scattering behavior cannot be reversibly transformed into the scattering behavior of an uncharged sample, hydrogen has to be bound irreversibly within the sample at this temperature and pressure. As will be shown in the following, this irreversible trapping of H is due to chemical bonding to excess-O at the M/O-interface. This H–O-bond is so strong that hydrogen remains within the sample even after an HV-annealing treatment.

To determine the bonding state of hydrogen to excess-oxygen at the interface, it is important to know that MgO-particles in Ag have a cube octahedral morphology [22,23]. An ideal cube octahedral consists of (1 1 1)- and (1 0 0)-facets in the ratio of 1:1. Assuming an oxygen-terminated (1 1 1)-oriented M/O-interface of the MgO, the corresponding theoretical occupancy of oxygen can be calculated to be $\Theta_{\mathrm{O}}^{(1\,1\,1)} = 1.3 \times 10^{15}\ \mathrm{cm}^{-2}$ for this interface. According to the structural model of Huang et al. [5] (see Fig. 1), the occupancy of the excess O should be half of this value, thus: $\Theta_{\mathrm{ExO}}^{(1\,1\,1)} = 0.5 \cdot \Theta_{\mathrm{O}}^{(1\,1\,1)} = 6.5 \times 10^{14}\ \mathrm{cm}^{-2}$ for the (1 1 1)-interface. In contrast to the (1 1 1)-interface, a terminating (1 0 0)-oriented interface consists of both, Mg-and O-ions. Therefore, there should be no excess-oxygen at these interfaces ($\Theta_{\mathrm{ExO}}^{(1\,0\,0)} = 0$). Finally, the (1 1 1):(1 0 0)-facet-ratio of 1:1 of the MgO-particles in Ag has to be taken into account. Hence, for the entire MgO-particle the theoretical occupancy density of excess oxygen is

$$\Theta_{\mathrm{ExO}} = 0.5 \cdot \Theta_{\mathrm{ExO}}^{(1\,0\,0)} + 0.5 \cdot \Theta_{\mathrm{ExO}}^{(1\,0\,0)} = 3.25 \times 10^{14}\ \mathrm{cm}^{-2}.$$

This value is in reasonable agreement with 2.2×10^{14} cm^{-2} as determined by gas volumetry [9]. The latter may be subject to larger error bars because the interfacial area was calculated using radii values determined from TEM micrographs revealing coffee bean contrast only and allowing to evaluate a small fraction of particles only.

Table 2
Comparison of the H-concentration $c_{\mathrm{H}}^{\mathrm{Inc.H}}$ determined via Eq. (4) from the incoherent scattering and the total number of H-traps at the M/O-interface according to Eq. (5)

R (nm)	$c_{\mathrm{H}}^{\mathrm{Inc.H}}$ (at.%)	$c_{\mathrm{H}}^{\mathrm{Interf.}}$ (at.%)
1.06 ± 0.01	0.58 ± 0.02	0.58 ± 0.03
1.61 ± 0.05	0.48 ± 0.03	0.44 ± 0.05
1.82 ± 0.06	0.48 ± 0.03	0.39 ± 0.04
2.17 ± 0.08	0.32 ± 0.03	0.33 ± 0.03
2.28 ± 0.08	0.32 ± 0.03	0.26 ± 0.03

Comparing this theoretical value of Θ_{ExO} with the hydrogen occupancy density of $\Theta_{\mathrm{H}} = (7.1 \pm 0.5) \times 10^{14}$ cm^{-2} determined by SANS-experiments shows $\Theta_{\mathrm{H}} \approx 2\Theta_{\mathrm{ExO}}$. This means that two hydrogen atoms were bound by one excess-oxygen atom at the M/O-interface. Since the SANS experiments show that one Ag-atom is displaced per one segregated H atom, it is straight forward to assume, that the excess-O, which undergoes significant charge transfer with Ag. Thus it can be considered as Ag_2O within the uncharged samples, and it forms an O–H-bond to H (or D) rather than maintaining the Ag–O-bond after hydrogen charging, because of the stronger chemical bond with hydrogen. The interface reaction could than proceed according to the following equation:

$$Ag_2O + H_2 \rightarrow H_2O + 2Ag \tag{11}$$

Alternatively, a formation of magnesium hydroxide is possible according to the reaction (cf. Fig. 1)

$$MgO + Ag_2O + H_2 \rightarrow Mg(OH)_2 + 2Ag \tag{12}$$

which explains the ratio of 2 H-atoms and 1 excess O-atom (bound as Ag_2O).

6. Summary

It has been proved by means of SANS that hydrogen segregates irreversibly at the internal metal/oxide-interfaces of the analyzed system. The absolute change of the macroscopic scattering cross-section $\mathrm{d}\Sigma/\mathrm{d}\Omega(Q)$ due to hydrogen charging increases with the total M/O-interfacial area and, therefore, increases with decreasing MgO-precipitate size. The H-occupancy density at the Ag/MgO-phase boundary has been determined to be $\Theta_{\mathrm{H}} = (7.1 \pm 0.5) \times 10^{14}$ H/cm^2. This amount is equal to half a monolayer of hydrogen around every MgO-particle. In addition, it could be shown that for each segregated hydrogen atom one silver atom is displaced from the M/O-interface. By comparing the hydrogen concentration with the number of hydrogen traps at the M/O-interface, it has been proved that nearly all hydrogen is located at the M/O-interfaces of the sample. In addition, hydrogen is trapped irreversibly at the M/O-particle interfaces. We explain these results by a reaction of hydrogen with excess-oxygen at the (1 1 1) M/O-interfaces of the MgO-particles. This excess-O, which has a weak bond to silver, bonds to hydrogen after H_2-loading and forms stronger OH-bonds. To the best of our knowledge, these are the first measurements that directly prove solute segregation at nano-size oxide particles by means of SANS. SANS allows to detect hydrogen which cannot easily be detected with other methods, and it provides the opportunity of performing powerful contrast experiments.

Acknowledgements

The authors are grateful for the financial support provided by the Deutsche Forschungsgemeinschaft through SFB 602 TP B1 and the financial as well as technical support for the SANS measurements at NIST by the National Science Foundation under Agreement No. DMR-9986442 and at Juelich, Germany, by the IFF, Forschungszentrum. We are also thankful for the collaboration with Terry Udovic and Juscelino Leão at NIST.

Appendix A

A short derivation of the macroscopic scattering cross-section of a segregated layer is given. In general (e.g. in [21]) the scattering cross-section is expressed by

$$\frac{\mathrm{d}\Sigma}{\mathrm{d}\Omega}(Q) = N\left|\int \Delta\rho \exp(-\mathrm{i}Qr)\,\mathrm{d}^3r\right|^2 = 16\pi^2 N|P(Q)|^2, \tag{A.1}$$

where N is the number of the scattering objects, $\Delta\rho$ the difference of the scattering length densities, e.g. number of scattered atoms times their coherent scattering length b_n per unit volume and Q is the scattering vector. It is possible to express the macroscopic scattering cross-section by the form factor of the scattered objects $P(Q)$ as defined via Eq. (A.1). In the following the form factor for spheres and spheres with an additional shell will be presented. The form factor of spheres $P(Q)|_{\mathrm{S}}$ is

$$P(Q)|_S = \Delta\rho_{\mathrm{SM}} \cdot f(R), \quad f(R) = \frac{\sin(QR) - QR\cos(QR)}{Q^3}, \tag{A.2}$$

$\Delta\rho_{\mathrm{PM}}$ is the difference of scattering length density of sphere and matrix and R the sphere- or particle-radius. By using this form factor for low Q-values, the following approximation is calculated according to Guinier:

$$\left.\frac{\mathrm{d}\Sigma}{\mathrm{d}\Omega}\right|_{\mathrm{S}}(Q) \cong \frac{16}{9}\pi^2 N \cdot R^6 \Delta\rho_{\mathrm{SM}}^2 \cdot \exp\left(-\frac{Q^2R^2}{5}\right). \tag{A.3}$$

For a sphere with an additional outer shell the form factor becomes

$$P(Q)|_{\mathrm{S+L}} = \Delta\rho_{\mathrm{L}} \cdot f(R+\delta R) - \Delta\rho_{\mathrm{L}} \cdot f(R) + \Delta\rho_{\mathrm{SM}} \cdot f(R) \tag{A.4}$$

with $\Delta\rho_{\mathrm{L}}$ as scattering length density of a shell of segregated atoms. Expanding $f(R+\delta R)$ in a Taylor series and neglecting quadratic contributions of δR leads to

$$P(Q)|_{\mathrm{S+L}} = \Delta\rho_{\mathrm{L}}\delta R\frac{\mathrm{d}f(R+\delta R)}{\mathrm{d}R} + \Delta\rho_{\mathrm{SM}} f(R).$$

Therefore, $\mathrm{d}\Sigma/\mathrm{d}\Omega(Q)$ becomes

$$\left.\frac{\mathrm{d}\Sigma}{\mathrm{d}\Omega}\right|_{\mathrm{S+L}}(Q) = 16\pi^2 N|P(Q)|^2 = 16\pi^2 N|\Delta\rho_{\mathrm{L}} \cdot f'(R) \cdot \delta R + \Delta\rho_{\mathrm{SM}} \cdot f(R)|^2.$$

Neglecting quadratic terms with δR^2 leads to

$$\left.\frac{\mathrm{d}\Sigma}{\mathrm{d}\Omega}\right|_{\mathrm{S+L}}(Q) \cong 16\pi^2 N[2\Delta\rho_{\mathrm{L}}\Delta\rho_{\mathrm{SM}}\delta R \cdot f'f + \Delta\rho_{\mathrm{SM}}^2 \cdot f^2]$$

with

$$\frac{\mathrm{d}f}{\mathrm{d}R} = \frac{Q^2R\sin(QR)}{Q^3}$$

and

$$f(R) = \frac{\sin(QR) - QR\cos(QR)}{Q^3},$$

the following equation is obtained:

$$\left.\frac{\mathrm{d}\Sigma}{\mathrm{d}\Omega}\right|_{\mathrm{S+L}}(Q) = 16\pi^2 N\Delta\rho_{\mathrm{SM}}2\delta R\Delta\rho_{\mathrm{L}}\frac{[Q^2R\sin QR][\sin QR - QR\cos QR] + \Delta\rho_{\mathrm{SM}}[\sin QR - QR\cos QR]^2}{Q^6}. \tag{A.5}$$

The net cross-section of a segregated layer is then calculated from the difference of Eqs. (A.5) and (A.3)

$$\left.\frac{\mathrm{d}\Sigma}{\mathrm{d}\Omega}\right|_{\mathrm{S+L}}(Q) - \left.\frac{\mathrm{d}\Sigma}{\mathrm{d}\Omega}\right|_{\mathrm{S}}(Q) = 16\pi^2 N\Delta\rho_{\mathrm{SM}}2\delta R\Delta\rho_{\mathrm{L}} \times \frac{[Q^2R\sin(QR)][\sin(QR) - QR\cos(QR)]}{Q^6}. \tag{A.6}$$

The first term decreases with Q^{-4} and the second term is oscillating around zero. For low Q-values, the following approximation is calculated for the Guinier-regime of the net cross-section of an outer shell:

$$\left.\frac{\mathrm{d}\Sigma}{\mathrm{d}\Omega}\right|_{\mathrm{L}}(Q) = \left.\frac{\mathrm{d}\Sigma}{\mathrm{d}\Omega}\right|_{\mathrm{S+L}}(Q) - \left.\frac{\mathrm{d}\Sigma}{\mathrm{d}\Omega}\right|_{\mathrm{S}}(Q) \cong \frac{32}{3}\pi^2 N\Delta\rho_{\mathrm{SM}}R^5\delta R\Delta\rho_{\mathrm{L}} \cdot \exp\left(-\frac{4Q^2R^2}{15}\right). \tag{A.7}$$

Finally, a normalized net cross-section $\mathrm{d}\Sigma/\mathrm{d}\Omega|_{\mathrm{L}}^0(Q)$ is given as the ratio of Eqs. (A.7) and (A.3)

$$\left.\frac{\mathrm{d}\Sigma}{\mathrm{d}\Omega}\right|_{\mathrm{L}}^0(Q) = \frac{6\Delta\rho_{\mathrm{Layer}}\delta R}{\Delta\rho_{\mathrm{SM}}R} \cdot \exp\left(-\frac{Q^2R^2}{15}\right). \tag{A.8}$$

References

[1] Oriani RA. Annu Rev Mater Sci 1978;8:327–57.
[2] Mader W. Z Metallkde 1989;80:139–51.
[3] Shashkov DA, Seidman DN. Phys Rev Lett 1995;75(2): 268–71.
[4] Wagner C. Z Elektrochem 1959;63:772.
[5] Huang XY, Mader W, Kirchheim R. Acta Metall Mater 1991;39:893–907.
[6] Backhaus-Ricoult M, Laurent S, Devaud J. J Phys IV 1999;9: 13.
[7] Backhaus-Ricoult M et al. Acta Mater 2000;48:4365.
[8] Pippel E, Woltersdorf J, Gegner J, Kirchheim R. Acta Mater 2000;48(10):2571–8.
[9] Gegner J, Hörz G, Kirchheim R. Interface Sci 1997;5:231.
[10] Kluthe C, Al-Kassab T, Kirchheim R. Mater Sci Eng A 2003;353(1–2):112–8.
[11] Kirchheim R. Prog Mater Sci 1988;32:262.
[12] Xiao SQ, Haasen P. Scr Met 1989;23:295, and 365.
[13] Alber U, Mullejans H, Rühle M. Acta Metall 1999;47(15–16):4047–60, 72.
[14] Blavette D, Cadel E, Fraczkiewicz A, Menand A. Science 1999;286:2317.
[15] Rüsing J, Sebastian JT, Hellman OC, Seidman DN. Microsc Microanal 2000;6(5):445–51.
[16] Sebastian JT, Seidman DN. Mater Res Soc 2001;654(12): AA4.9.1–6.
[17] Heuser BJ, King JS, Summerfield GS, Boué F, Epperson JE. Acta Metall Mater 1991;39:2815.
[18] Kirchheim R, Huang XY, Carstanjen H-D, Rush JJ, Glinka J, Petry A. Z Phys Chem NF 1989;163:203.
[19] Maxelon M, Pundt A, Pyckhout-Hintzen W, Barker J, Kirchheim R. Acta Mater 2001;49:2625.
[20] Kluthe C, Al-Kassab T, Kirchheim R. Mater Sci Eng A 2002;327:70–5.
[21] Porod G. In: Glatter O, Kratky O, editors. Small-angle X-ray scattering. New York: Academic Press; 1983.
[22] J. Gegner, Segregation v. Sauerstoff an inneren M/O-Phasengrenzen. PhD thesis, MPI, Stuttgart; 1995.
[23] Mader W, Maier B. Coll Phys 1990;51:867.
[24] Raub E. In: Fromm E, Gebhardt E, editors. Gase u Kohlenstoff in Metallen. Berlin: Springer; 1976. p. 678.